Topobathymetric 3D model reconstruction of shallow water bodies through remote sensing, GPS, and bathymetry

Reconstrucción de modelo 3D topobatimétrico de cuerpos de agua someros mediante teledetección, GPS y batimetría

Hugo Luis Rojas-Villalobos[1,6], Luis Carlos Alatorre-Cejudo[2], Blair Stringam[3], Zohrab Samani[4] and Christopher Brown[5]

Recibido: Enero 6, 2018 *Aceptado: Noviembre 11, 2018*

Abstract

Since there are no mathematical models that can calculate the Laguna de Bustillos' water storage levels, water balance requires this data to understand the connectivity between this water body and the Cuauhtemoc aquifer. This article presents a new three-dimensional reconstruction technique based on a time series of multispectral remote sensing images, bathymetry, a topographic survey with high precision GPS, and regional contours. With the images of Landsat ETM+/OLI and Sentinel 2A from 2012 to 2013, 2016, and 2017, the contours of the water surface were extracted using the MNDWI and were associated with an elevation received from GPS. An Autonomous Surface Vehicle was also used to obtain the bathymetry of the lake. A topographic survey was carried out using GPS in populated areas, and the contour lines extracted from the INEGI Continuous Elevations Model 3.0. A DEM was constructed using ArcGIS 10.5.1, and surfaces and volumes were calculated at different elevations and compared with 16 Landsat TM/ETM+/OLI multispectral images from 1999 to 2018. The results showed that the mean of the average intersection area between the test images and the area extracted from the 3D model is above 90.9% according to the confidence interval, kappa overall accuracy 95.2–99.7%, and a coefficient 89.9–99.3%. This model proved to be very accurate on a regional scale when the water level exceeded 1971.32 meters above mean sea level and useful to evaluate and administer water resources.

Palabras clave: DEM, storage, lake, MNDWI, RTK, sound.

Resumen

Ante la inexistencia de modelos matemáticos que calculan el almacenamiento de agua de Laguna de Bustillos, el balance hídrico requiere este dato para comprender la conectividad entre este cuerpo de agua y el acuífero Cuauhtémoc. Este artículo presenta una nueva técnica de reconstrucción tridimensional basada en series de tiempo de imágenes de sensores remotos multiespectrales, batimetría, levantamiento topográfico con GPS de alta precisión y curvas de nivel regionales. Con las imágenes de Landsat ETM +/OLI y Sentinel 2A de 2012 a 2013, 2016 y 2017, se extrajeron los contornos de la superficie del agua utilizando el MNDWI y se asociaron con una elevación obtenida a través del GPS. Se utilizó un Vehículo Autónomo de Superficie para obtener la batimetría del lago. Se realizó un levantamiento topográfico usando GPS en áreas pobladas y se usaron las curvas de nivel extraídas del Modelo 3.0 de Elevaciones Continuas del INEGI. Se construyó un MDE, las superficies y volúmenes se calcularon a diferentes elevaciones y se compararon con 16 imágenes multiespectrales Landsat TM/ETM+/OLI de 1999 al 2018. Los resultados mostraron que la media del área promedio de intersección del modelo y las imágenes tiene una eficiencia superior al 90,9% de acuerdo con el IC, precisión general kappa 95.2-99.7% y un coeficiente 89.9-99.3%. Este modelo demostró ser muy preciso en escala regional, sobre todo cuando el espejo del agua supera los 1971.32 metros sobre el nivel medio del mar, y a la vez útil para la evaluación y administración de los recursos hídricos.

Keywords: MDE, almacenamiento, lago, MNDWI, RTK, sonar.

[1] New Mexico State University. Water Science and Management Program. Department of Geography, 1525 Stewart St. Breland Hall, Las Cruces, NM. USA. 88003. Tel. (+1 575) 646-5755.
[2] Universidad Autónoma de Ciudad Juárez, Sede Cuauhtémoc. Programa de Geoinformática, Departamento de Arquitectura. Carretera Anáhuac S/N, Cd. Cuauhtemoc, Chih, México. 31600. (+52 625) 128-1700.
[3] New Mexico State University. Plant and Environmental Sciences. College of Agriculture, Consumer and Environmental Sciences, 945 College Drive. Skeen Hall, Las Cruces, NM. USA. 88003. (+1 575) 646-7665
[4] New Mexico State University. Department of Civil Engineering, 3035 S. Espina St. Hernandez Hall, Las Cruces, NM. USA. 88003. (+1 575) 646-2904
[5] New Mexico State University. Department of Geography, 1525 Stewart St. Breland Hall, Las Cruces, NM. USA. 88003. Tel (+1 575) 646-1892.
[6] Dirección electrónica del autor de correspondencia: hlrojas@nmsu.edu

Introduction

The Laguna de Bustillos is in a region that has a high demand for groundwater for the agricultural industry, making the Cuauhtemoc aquifer the largest over-exploited aquifer in northwest Mexico (Comisión Nacional del Agua, 2016). It is necessary to provide updated data to the water balance of the basin to improve water management in the region.

Because there are no known mathematical models that calculate water storage, it is imperative to develop a new technique or method that allows us to estimate the water volume contained in water bodies. The calculation of water storage of shallow water bodies requires the construction of 3D models of the terrain including the surrounding areas. Integrating techniques based on sound, spectral analysis of satellite imagery, and GPS allow researchers to increase the accuracy of the existing 3D models and expand them from the reservoir representation to a topobathymetric integrated model.

Topobathymetry is a geospatial concept that integrates bathymetric and topographic data from different spatial scales, time, and sensors. The terrain model is applied to monitor coastal erosion, sea level rise, flood impact reduction programs, and coral barrier studies (Gesch *et al.,* 2016). Digital terrain models, topography, bathymetry, and the use of water body contours are essential sources for integrating this model. Some research tried to get 3D models, but only one or two data sources were used in comparison with those applied in this research. The delimitation of water bodies is an indirect way of getting contour lines through differentiating the spectral response between the green band (G) and the bands near infra-red (NIR) or the infra-red short-wave band (SWIR). The Normalized Difference Water Index (NDWI) (McFeeters, 1996) and the Modification of Normalized Difference Water Index (MNDWI) (Xu, 2006) have been used to monitor (Lu *et al.,* 2013) changes in the extent of the lakes (Ma *et al.,* 2007), and the location of water bodies (Rana and Neeru, 2017). Sonar is a technique that uses sound waves to calculate water depth (Knott and Hersey, 1957) and has advantages such as high accuracy (± 0.1 m), low cost, and the device can be mounted on any boat. Several types of research have used sound for mapping water bodies (McPherson *et al.,* 2011; Popielarczyk and Templin, 2014; Giordano *et al.,* 2015). Leon and Cohen (2012) modeled the volume of Lake Eyre in Australia using bathymetry and remote sensing. The authors used surveys realized in 1974 and 1976 with the precision of ± 0.3 m in the vertical component and up to ± 500 m in the horizontal component, which proved to be a very limited and inaccurate method.

Water storage has two components: groundwater and surface water (lakes, ponds, or reservoirs) (Brooks *et al.,* 2012). Some variations in water storage in the reservoirs are due to an underground hydraulic connection between aquifers and water bodies (Isiorho *et al.,* 1996; Winter, 1999). These variations in the volume of water can be so drastic that large reservoirs dry up in a short time like Laguna de Bustillos had in years 2002 to 2006 and 2013 (NASA, 2017). Although there is a geohydrological study that supports recharge deficit in the aquifer, there is no information about the storage capacity of Laguna de Bustillos. The lack of information encourages the main objective of this research to generate a new technique to generate a 3D topobathymetric model that contributes to the generation of updated data, which allows the deduction of variables, such as underground infiltration from the catchment area of Laguna de Bustillos. Despite these models of volumetric estimation of water bodies, the combination of more than two different topobathymetric measurement techniques had not been explored. This document proposes a unpublish new method integrating three methodologies to generate a more robust and accurate three-dimensional model.

Materials and methods

This study was conducted between 2016 and the first semester of 2018 in the Spatial Applications and Research Center at the New Mexico State University. The study area of Laguna de Bustillos is in the quadrant between the coordinates 28° 38' 51'' N – 28° 28' 27'' N and 106° 57' 3'' W – 106° 38' 50'' W in the municipality

Figure 1. The study area of Laguna de Bustillos, Chihuahua. Source: LandsatLook Viewer (USGS, 2017a).

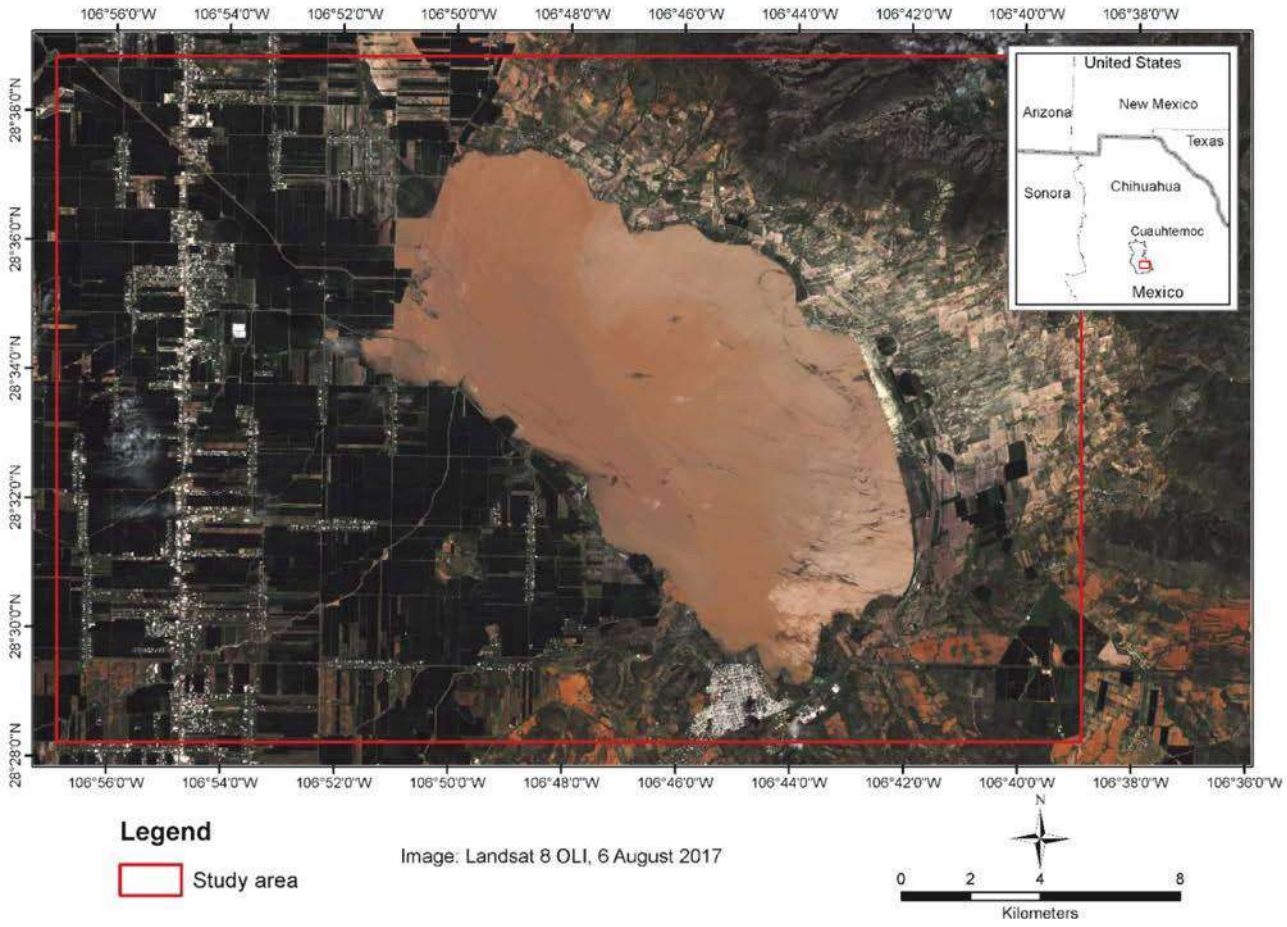

of Cuauhtemoc, in the state of Chihuahua (Figure 1). This region's climate is warm and semi-arid since it is in a transition zone between the semi-humid climate of the mountains and the Chihuahua desert (Kottek *et al.,* 2006). The average annual temperature ranges from 6.9 to 21°C, with an average annual rainfall of about 528 mm per year (Servicio Meteorológico Nacional, 2017).

The authors designed a new four-stage method to develop a 3-D topobathymetric model for the purpose of determining water storage: i) extract contour lines through a time series of remote sensing; ii) determine bathymetry; iii) perform a topographic survey (GPS-RTK); and iv) extract contours from the regional terrain digital model. Also, it was included a regression analysis in determining the two equations that provide the volume and surface area using water height. The flowchart below (Figure 2) shows the modeling process.

Bathymetry

The New Mexico Water Resources Research Institute (WRRI) funded a project to build an Autonomous Surface Vehicle (ASV) to generate bathymetric data for shallow water bodies. A PVC center frame was attached to a two-hulled catamaran boat, propelled by two motors, and equipped with a GPS on the top to receive signals via satellite to provide the direction and location. An Ardupilot® system automated the catamaran navigation through an Arduino® MEGA 2560 board to receive the GPS signal while the sonar data bus decoded and recorded the information on an SD card. Subsequently, the recorded points were downloaded to a computer for processing. The transducer was a Garmin® Intelliducer Thru-Hull NMEA-0183, which does not require the previous calibration and can measure from 60 cm to 200 m with a 0.1 m accuracy (Rojas-Villalobos, 2016).

Figure 2. Schematic of the workflow to generate the 3D model.

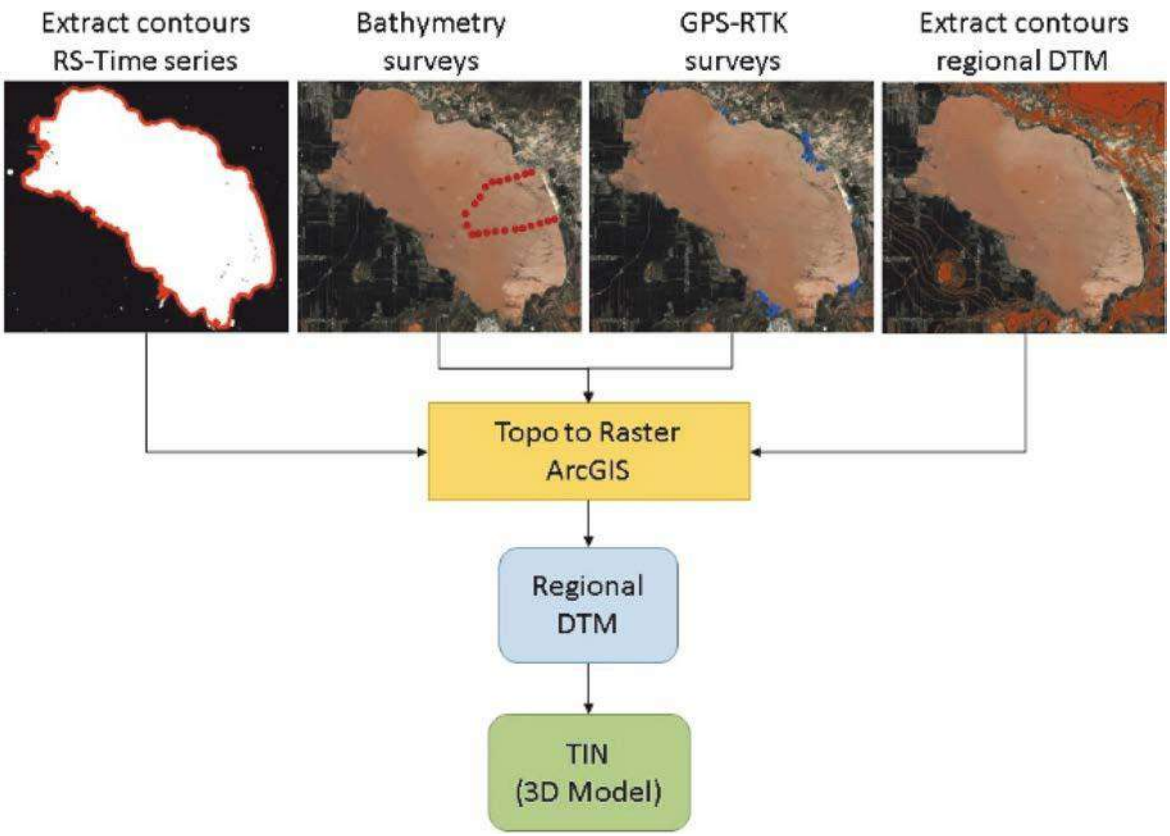

Figure 3. Components to calculate the height of the lake bottom above sea level.

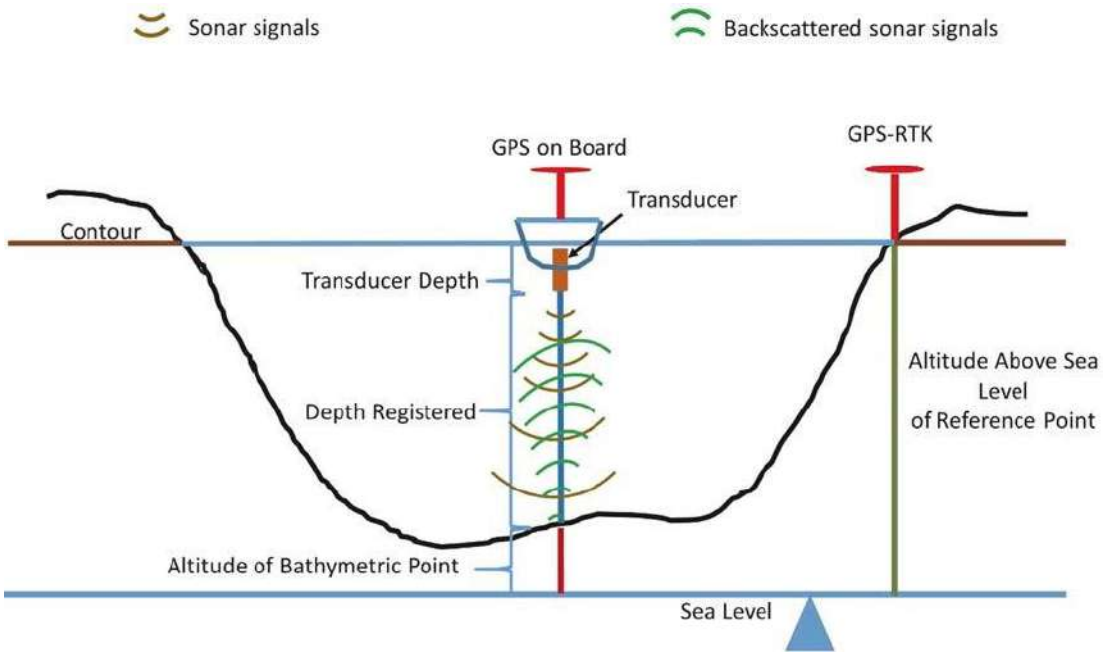

To construct a 3D model of the region including the bottom of the lake, the bathymetry data (depth) was transformed into topographic data (height). Figure 3 shows the schematic of the surveying process to transform to the correct topographic points.

The following equation (1) was developed to calculate the altitude above sea level for each bathymetric point:

$$APB = ASNM - (PS + PR) \quad (1)$$

Here, ABP is the height of the bathymetric point, ASNM is the altitude above sea level of the reference level, PS is the depth of the sonar, and PR is the recorded depth. The bathymetry consisted of 5 trajectories, and the data were adjusted through the above equation using the reference levels of the survey days. A GPS-RTK was used to establish the fixed reference point corresponding to the height of the lake contour and was linked to the bathymetry obtained that day.

Contour extraction from remote sensors

Since the spatial resolution of remote sensing is the most important factor for delineating the contours of water bodies, Landsat ETM +, Landsat OLI (Operational Land and Imager), and Sentinel 2A (Table 1) were chosen to build the MNDWI.

These images are available for free on the LandsatLook Viewer websites of the United States Geological Survey (USGS, 2017a) and the Copernicus Open Access Hub of the European Space Agency (ESA, 2017). Seven images were selected with the lowest possible cloudiness over the study area during the time the lake had gradually dried (March 2012 – August 2013). Also, six recent images were downloaded to establish the maximum lagoon extent and baseline curves for the bathymetry data (June 2016 – September 2017). Using the Semiautomatic Classification extension (Congedo, 2013) in QGIS®, atmospheric correction was applied to the images using the method of Subtraction of Dark Objects 1 (Chavez, 1996). Then, a fusion of images was performed with the panchromatic band (ETM + and OLI) using the Brovey transformation (Johnson *et al.,* 2012) to increase the spatial resolution to 15 m before the MNDWI construction.

The Normalized Difference Water Index (NDWI) was created to identify Landsat water bodies. The high relative reflectance of green (G) in the electromagnetic spectrum contrasts with the high absorption of the NIR in clear water (McFeeters, 1996). Excessive suspended matter in the water increases reflectance measurements in the NIR band (Ruddick *et al.,* 2006), thus dramatically reducing the difference between the G-NIR bands, which makes it difficult to distinguish between water and non-water surfaces.

Table 1. Collection of remote sensing data used in this article.

Sensor	Acquisition date	Bands (μm)	Spatial resolution (m)
Landsat ETM+	19 May 2012; 4 June 2012;	2 (Green 0.52-0.60)	30
(USGS, 2017a)	20 June 2012; 14 January 2013;	5 (SWIR-1 1.55-1.75)	30
	6 February 2013; 22 February 2013	8 (Panchromatic)	15
Landsat OLI	2 August 2013; 14 June 2016,	3 (Green 0.533-0.590)	30
(USGS, 2017a)	29 August 2017; 5 September 2017	6 (SWIR1 1.566-1.651)	30
		8 (Panchromatic 0.503-0.676)	15
Sentinel 2A	20 March 2017; 8 June 2017	3 (Green 0.542-0.577)	10
(ESA, 2017)	6 August 2017	11 (SWIR1 1.568-1.658)	20

Therefore, the NDWI method is not fit for Laguna de Bustillos due to the turbidity of water. The MNDWI suppresses this problem by replacing the NIR band with an infrared shortwave band (SWIR) because the water absorbs energy and the reflectance is low. The equation that determines the MNDWI (Xu, 2006) is:

$$MNDWI = \frac{G - SWIR}{G + SWIR} \quad (2)$$

Where G is the green band of the electromagnetic spectrum and SWIR is the short-wave band of the infrared spectrum. The possible MNDWI values are from -1 to 1.

In ArcGIS®, the raster calculator was used to apply the MNDWI equation to Landsat and Sentinel images. According to the MNDWI method, positive values represent water and negative values the surface without water. Therefore, the resulting raster was reclassified by assigning 1 to those values greater than 0 and 0 to values less than or equal to 0. From the reclassified images, the contours were extracted and examined through visual interpretation. This procedure ensures that the extracted contours correspond to the edge of the lake using false infrared color composite images and avoids errors due to the influence of the vegetation.

A failure of the SLC (Scan Line Corrector) introduced strips with missing data in the Landsat ETM+ images captured on May 31st, 2003 (USGS, 2017b). Due to this error in the sensor, only segments were vectorized corresponding to the edge of the water surface.

An orthometric height was assigned to the contours using the closest ABP to the contour line (< 0.5 meters). When there were no bathymetry points near the line, points were selected in a buffer of 1 to 2 m on each side of each contour. The contour took the mean height following the Classic Central Limit Theorem (Erdös and Rényi, 1959; Dowdy *et al.,* 2011). According to this theorem, when the sample size increases, the average sample will approximate a normal distribution. This procedure reduces the uncertainty and variability of bathymetric data due to boat sway and sonar accuracy (Krause and Menard, 1965; Eltert and Molyneux, 1972; Schmitt *et al.,* 2008).

Topography

The GPS points were measured using two SOKKIA GRX2 GNSS devices with a horizontal accuracy of 5 mm and 10 mm on the vertical axis. A GPS was established as base at the coordinate 28° 27' 25.1532" N and 106° 47' 24.9432" O at the height of 2069.08 on the WGS ellipsoid of 1984. 1006 topographic points were collected and transformed to the Mexican Gravimetric Geoid 2010 (GGM10) to generate altitude above the mean sea level (INEGI, 2015).

Digital elevation model

A contour was extracted at every meter from the Mexican Elevation Continuation 3.0 (CEM 3.0) of the National Institute of Statistics and Geography (INEGI, 2016). On September 5th, 2017, the water level of the lake was 1975.56 m above sea level (masl). For this reason, contour lines below 1976 m were eliminated from the regional DEM.

Topobathymetric 3D model and volume estimation

An MDE with a spatial resolution of 2 m was created using the four sources of elevation data using the Topo-to-Raster tool contained in the 3D analysis module of ArcGIS. This tool allows the creation of hydrologically correct lifting meshes based on the ANUDEM program (Hutchinson *et al.,* 2011). Since the triangulated irregular network (TIN) generates more accurate volumetric calculations (Mi *et al.,* 2007; Hanjianga *et al.,* 2008), the DEM was converted into a TIN. The volume and water surface were calculated from 1970.50 m to 1978.9 masl every 1 mm using the *ArcGIS Polygon Volume* tool.

Statistical Evaluation

Since there is no previous model to evaluate the lake storage, 16 areas of water coverage of different scenes were extracted through remote sensing (RS) when the lake was drying (real area) (Table 2).

The area of each scene was used to extract the corresponding contour line from the 3D model and generate the area. Using ArcGIS, the intersection of the two layers was the area of a coincidence that was statistically evaluated (Figure 4).

Table 2. List of multispectral images used to compare 3D model contours.

Sensor	Acquisition date	Water surface (km²)
Landsat TM (USGS, 2017a)	25 June 1999	99,585,900
	26 May 2000	92,322,000
	11 June 2000	90,583,200
	17 March 2001	77,341,500
	2 April 2001	70,556,400
	27 Abril 2001	64,676,700
	24 November 2002	41,630,400
	15 September 2003	64,507,500
	21 December 2006	109,260,000
Landsat ETM+ (USGS, 2017a)	27 January 2000	104,792,438
	5 May 2001	61,820,100
	28 August 2002	68,073,300
Landsat OLI (USGS, 2017a)	1 May 2014	87,509,700
	2 June 2014	79,517,700
	28 August 2014	109,547,000
	8 October 2014	118,406,700

Figure 4. Demonstration of matching areas between water surface extracted from a multispectral satellite image and the 3D model at the same reference level.

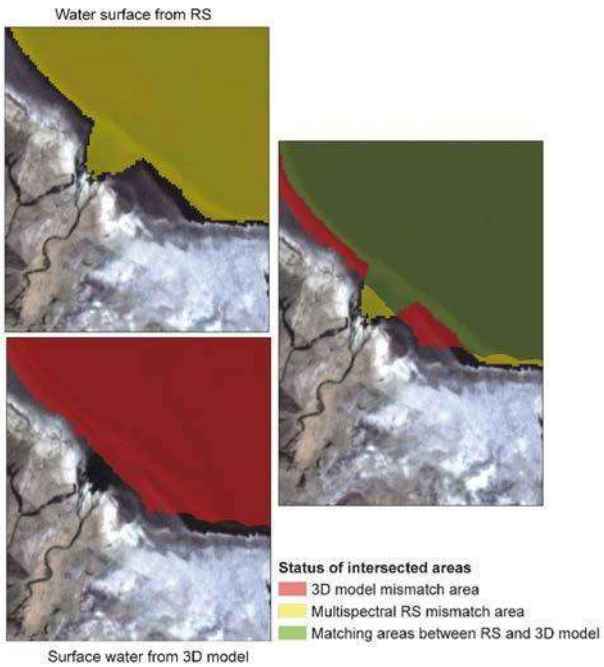

Some Landsat ETM + and OLI images were replaced with recent Sentinel 2 images (early 2018) to distribute the extracted contours along the height through the 3D model (Table 3). This procedure is used to evaluate the model accuracy (reality vs. model).

Table 3. List of multispectral images used to compare areas between reality and 3D model. Added images are identified with *.

Sensor	Acquisition date	Water surface (km²)
Landsat TM (USGS, 2017a)	25 June 1999	99,585,900
	26 May 2000	92,322,000
	11 June 2000	90,583,200
	17 March 2001	77,341,500
	2 April 2001	70,556,400
Landsat ETM+ (USGS, 2017a)	27 January 2000	104,792,438
	5 May 2001	61,820,100
	28 August 2002	68,073,300
Sentinel 2 (ESA, 2017)	4 May 2016*	109,321,000
	23 July 2016*	105,033,000
	14 January 2018*	133,912,000
	4 April 2018*	131,504,000

Because of the surface area changes according to the elevation of the water surface, it is not possible to evaluate the efficiency of the model directly. For this reason, the relationship between the coincidence surface and the reference area of the satellite image were used.

The maximum possible relation between both areas is 100% because the level curves obtained from the 3D model are directly related to the waterbody contours. The water/non-water coverage maps of the model and the satellite images of each year (Table 3) were analyzed using the Kappa statistic (K-hat) through QGIS (QGIS, 2018) and Semi-Automated Classification Plugin (Congedo, 2013). The Kappa coefficient and overall accuracy allows us to know the degree of agreement between the 3D model and the water body surface (Card, 1982; Jensen, 2007; Congalton and Green, 2008; Lillesand *et al.,* 2014) . Also, the t-statistical distribution was applied to find the lower limit of the 95% Confidence Interval and estimated the range of acceptable match surface values (from Table 2) according to the sample mean (Dowdy *et al.,* 2011) (3).

$$IC_{0.95} = \bar{x} - t_{\alpha,v}\frac{s}{\sqrt{n}} \quad (3)$$

Where $\bar{x}$ is the mean of the sample, α is the level of significance, v is the degrees of freedom (n -1), s is the standard deviation, and n is the sample size.

Finally, two equations were generated representing the area of the water surface and the volume contained in the lake according to the elevation of the water surface.

Results and discussion

Figure 5 shows the sources of data used for the reconstruction of the topobathymetric model: 13 contours from remote sensors, 29,715 bathymetry points, 1,006 GPS points, and INEGI contours.

Figure 5. Map showing bathymetry, GPS points, derived curves from multispectral RS, and regional contours (INEGI).

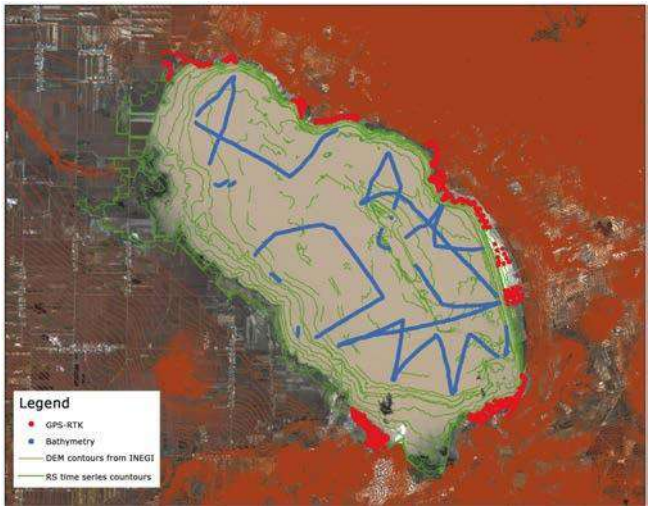

Figure 6. Triangulated Irregular Network is representing the topobathymetric 3D model of Laguna de Bustillos.

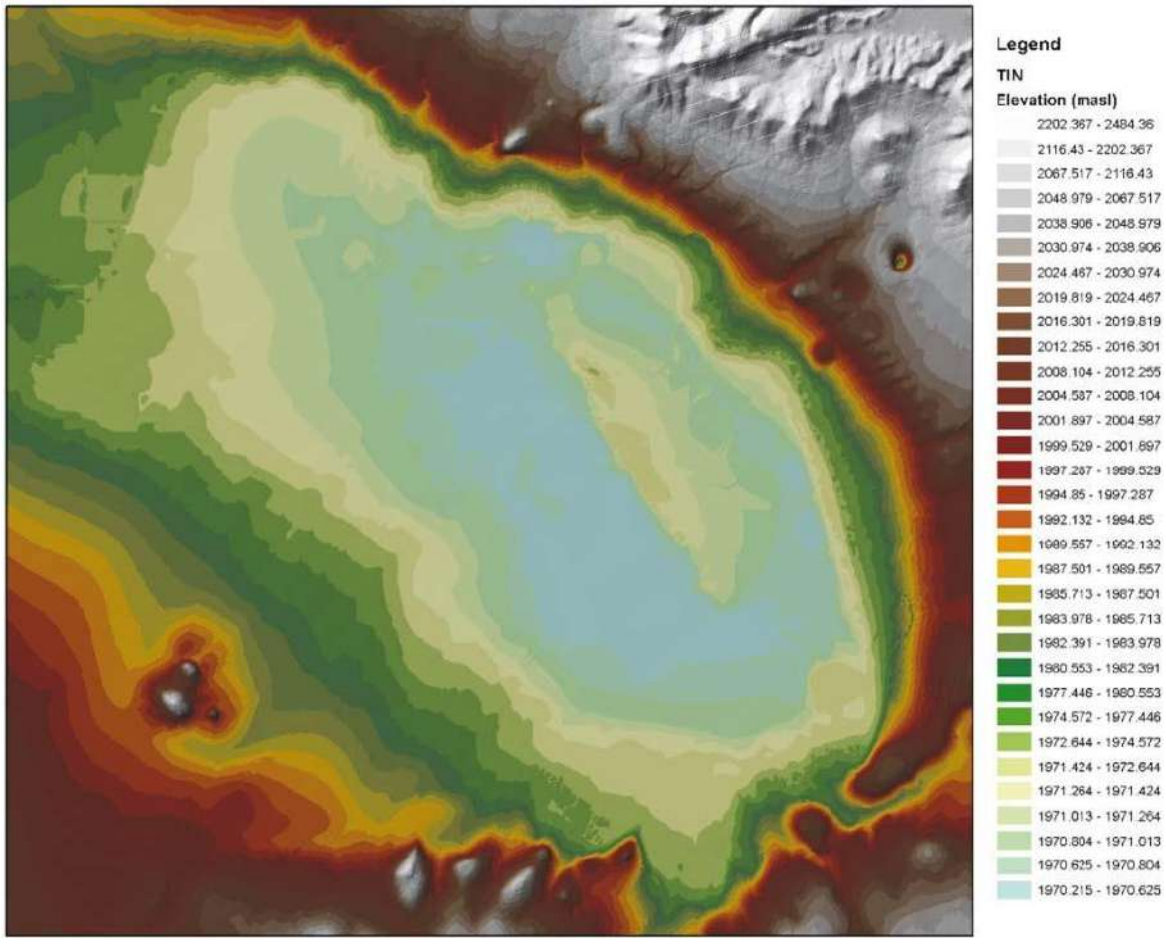

As a result of the reconstruction data process, Figures 6 and 7 show the 3D topobathymetric model and a 3D perspective of the Laguna de Bustillos. The results show that the deepest point of the lake is at 1970.215 masl, the maximum depth is 3.785 m when the water level reaches the 1974 masl, the water storage is 324.4 Mm^3, and the average depth is 1.37 m.

Figure 7. 3D perspective of Laguna de Bustillos (5 times height exaggeration for better visualization).

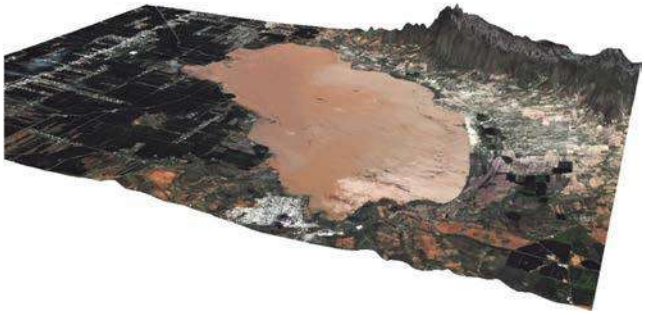

Since the Kappa statistic shows the difference between classified values of the satellite image (reference data) and the surface of water body generated by the 3D model, the coincidence is expected to be high. Typically, Kappa values greater than 0.80 represent a strong match between the compared data. The result of the comparison shows an overall accuracy higher than 95.21% and the K-hat coefficients above 0.899. Table 4 shows the increase of the values of overall accuracy and the Kappa coefficient when the water level is higher.

It is observed that the values of elevation that are between 1971.168 and 1971.284 have a value of K-hat less than 0.9289 and are associated with water coverage less than 80 km^2. When the water level rises above 1971.284 m, the Kappa indicator increases its value above 0.93, reaching levels of 0.99. Also, low K-hat values (0.8993 – 0.9289) are associated with low depth averages (<0.41 m) in contrast to those K-hat values above 0.96 that are in depth averages greater than 0.71 m.

Table 4. Kappa coefficient values and overall accuracy between imagery (reality) and simulation (3d model).

Date	Sensor	Surface (km^2)	Elevation (m)	Depth Average (m)	K-hat	Overall Accuracy (%)
25/06/1999	Landsat TM	99.59	1971.713	0.710	0.9627	98.150
27/01/2000	Landsat ETM+	104.86	1972.034	0.987	0.9669	98.383
26/05/2000	Landsat TM	92.32	1971.460	0.501	0.9347	96.738
11/06/2000	Landsat TM	90.58	1971.442	0.493	0.9316	96.582
17/03/2001	Landsat TM	77.35	1971.284	0.409	0.9079	95.499
02/04/2001	Landsat TM	70.56	1971.235	0.397	0.8993	95.212
05/05/2001	Landsat ETM+	61.82	1971.168	0.383	0.8993	95.480
28/08/2002	Landsat ETM+	68.07	1971.228	0.405	0.9289	96.669
04/05/2016	Sentinel 2	109.32	1972.809	1.709	0.9939	99.710
23/07/2016	Sentinel 2	105.03	1972.050	1.000	0.9883	99.430
14/01/2018	Sentinel 2	133.91	1975.857	4.195	0.9787	99.171
04/04/2018	Sentinel 2	131.55	1975.554	3.955	0.9687	98.750

Conversely, with a confidence level of 95%, the mean of the percentage of matching areas between the satellite images and the 3D model is greater than 90.9% (Table 5).

Table 5. Confidence Interval analysis for the percentage of the matching area between the three-dimensional model and the sample images.

Mean	0.934663471	**Degree of freedom**	15
Standard Error	0.0145891	**α**	0.05
Median	0.954318	**$t_{0.05,15}$**	1.753
Standard deviation	0.0583564	**$t_{0.05,15}$ Std. Error**	0.025574712
Simple variance	0.0034055	**$IC_{0.95}$: $\bar{X}$ - $t_{0.05,15}$ Std. Error**	0.9090888
Sample size	16		

Below the contour 1971.325 m, four of the six comparisons are below the lower limit of the confidence interval (Figure 8).

Figure 8. Graph showing the behavior of the intersection percentage between the surfaces of the 3D model and the areas of RS images along elevation.

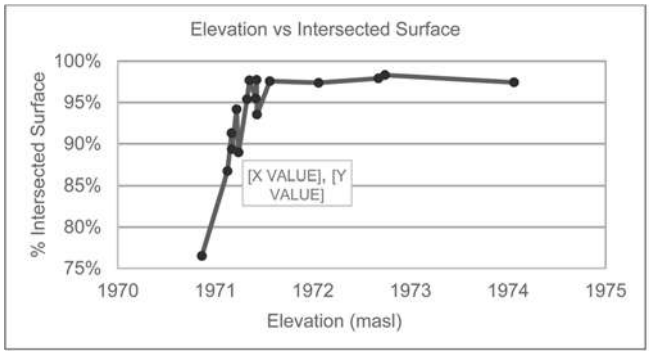

The mean area intersected below the reference level is only 88.91%, while in the upper range, it is 97.01%.

Two equations were generated that estimated the area of water coverage according to the depth of the lake. The first equation calculated the volume below the 1971.325 masl and the second equation calculated the remaining volume above it. Similarly, two other equations were generated estimating the amount of water in the lake. The determination coefficients (R^2) for the estimated equations are greater than 0.9882; this indicates that the equations obtained are suitable for the topobathymetric model within the extent limits of the lake (Figure 9).

Figure 9. Graphs of the surface and volume equations adjusted to the 3D model.

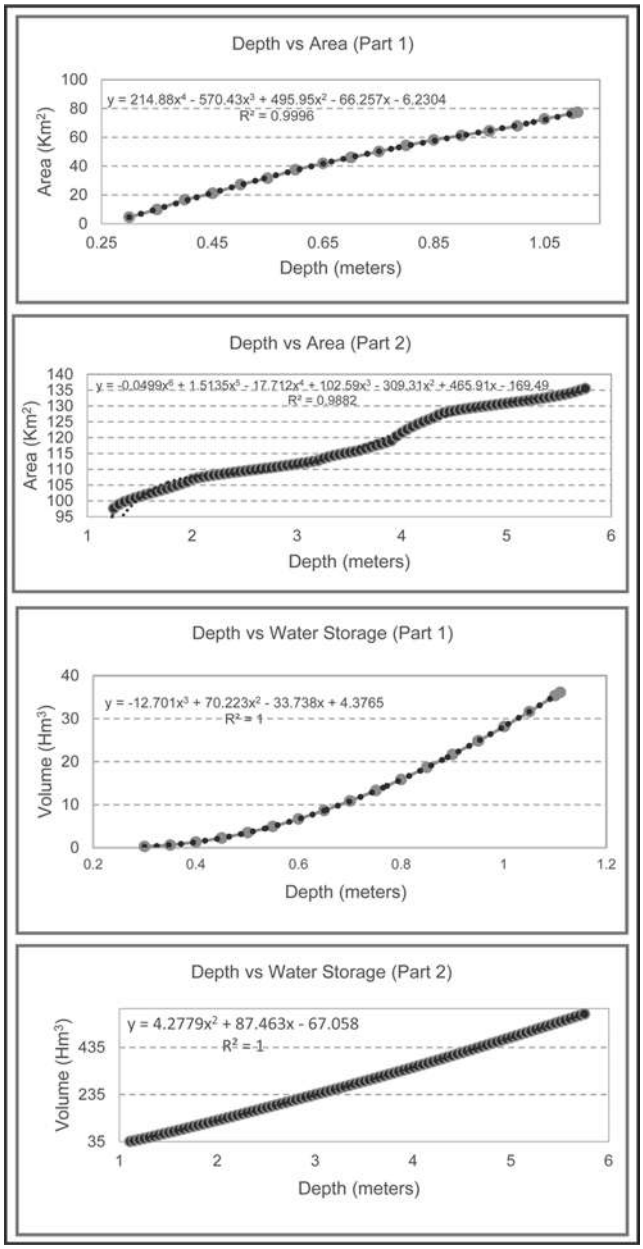

Conclusions

Four different techniques, such as bathymetry, GPS-RTK points, and contour lines extracted from the remote sensors, were decisive in creating this new three-dimensional modeling methodology for water bodies. Its efficiency is demonstrated after the statistical analysis applied. According to the results obtained in the Kappa analysis and the confidence interval, the 3D model is a robust and precise model (Kappa>0.80).

Three processes were important in the construction of the model:

· The use of high precision GPS helped in fixing the reference height points of the contours of the most recent satellite images (2015 – 2018) with great precision and accuracy.

· The bathymetric points linked to the current height of the water level of the lake were instrumental in establishing the height above sea level at the bottom of the lagoon.

· The related height between the bathymetric points and the levels closest to the bottom of the lake was extracted from the satellite images (1999 – 2002).

Additionally, it was observed that the segments of the contours extracted from the Landsat ETM+ images with an error in the SLC (USGS, 2017b) influenced the relative low efficiency (0.8993 < Kappa <0.9079) of the model below 1971.325 masl. On the other hand, effectiveness in the top height ranges from 1971.5 to 1974 masl was as a result of the spatial resolution of the satellite images of Landsat OLI (15 m panchromatic) and Sentinel 2 (10 m) (Figure 10).

Although this 3D hydrological model is very robust to be used in the administration of water in the basin, special care must be taken in forecasting floods in rural-urban areas. The model simulates much of the flooded areas of Mennonite farmers, but the 3D model should not be used to prevent flood risks due to the topographic complexity with dams and ditches.

In future work, researchers should continue the bathymetric survey with greater data density using a sonar with increased accuracy to further the model's efficiency. The acquisition of more bathymetric data will allow replacing contours extracted from the oldest images such as Landsat ET and ETM +. Additionally, the photogrammetric triangulation could be of great benefit in urban and agricultural zones to delineate more accurate topography. This development is the first step to estimate the volume of water in the Laguna de Bustillos as this work produces estimates that approximate the actual values and such research is relevant to water management in the region.

Figure 10. RS time series contours. The dark contour delimits the outer areas with greater 3D model performance and the internal area with less accuracy.

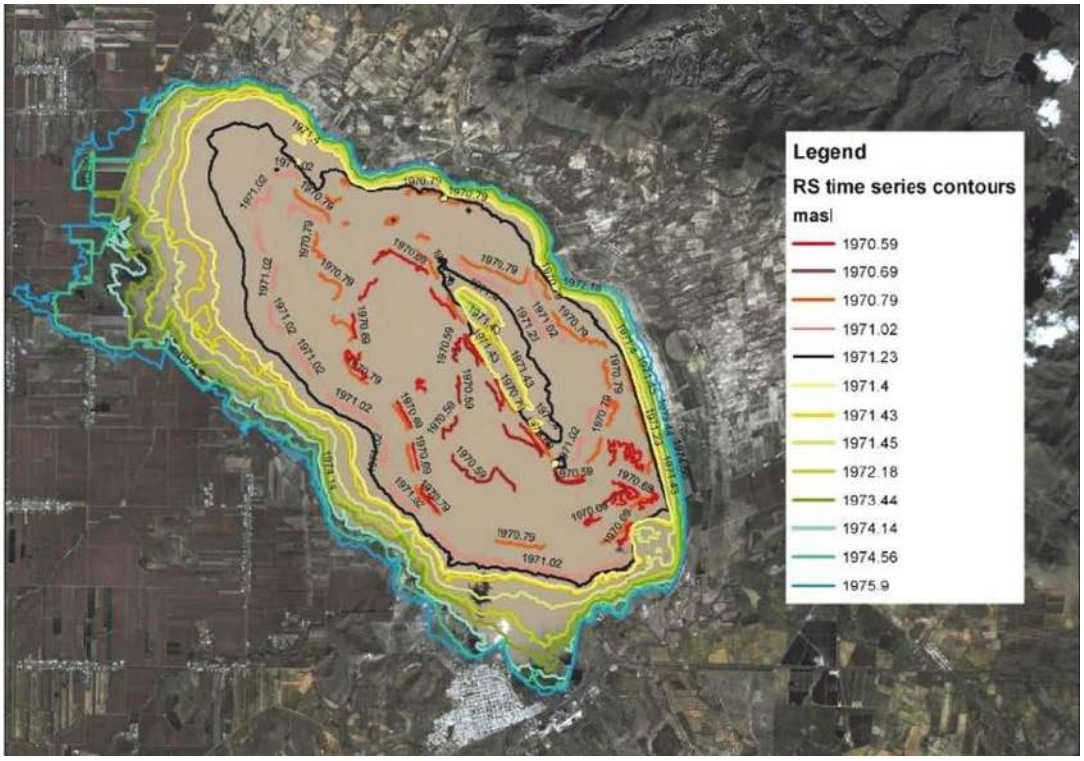

Literature cited

Brooks, K.N., P.F. Ffolliott, and J.A. Magner 2012. Hydrology and the Management of Watersheds. John Wiley & Sons. Iowa. 533 p.

Card, D.H. 1982. Using known map category marginal frequencies to improve estimates of thematic map accuracy. *Photogramm. Eng. Remote Sens 48*: 431–439.

Chavez, P.S. 1996. Image-based atmospheric corrections-revisited and improved. *Photogramm. Eng. Remote Sens 62*: 1025–1035.

Comisión Nacional del Agua, 2016. Estadísticas del agua en México. Secretaría de Medio Ambiente y Recursos Naturales, México.

Congalton, R.G., Green, K., 2008. Assessing the accuracy of remotely sensed data: principles and practices. CRC press.

Congedo, L., 2013. Semi-automatic classification plugin for QGIS. Sapienza Univ. Rome.

Dowdy, S., Wearden, S., Chilko, D., 2011. Statistics for Research. John Wiley & Sons.

Eltert, J.F., Molyneux, J.E., 1972. The long-distance propagation of shallow water waves over an ocean of random depth. *J. Fluid Mech 53*: 1–15.

Erdös, P., Rényi, A., 1959. On the central limit theorem for samples from a finite population. Publ Math Inst Hung. *Acad Sci 4*: 49–61.

ESA, 2017. Copernicus Open Access Hub [WWW Document]. URL https://scihub.copernicus.eu/ (accessed 8.23.17).

Gesch, D.B., Brock, J.C., Parrish, C.E., Rogers, J.N., Wright, C.W., 2016. Introduction: Special Issue on Advances in Topobathymetric Mapping, Models, and Applications. *J. Coast. Res 76*: 1–3.

Giordano, F., Mattei, G., Parente, C., Peluso, F., Santamaria, R., 2015. MicroVeGA (micro vessel for geodetics application): A marine drone for the acquisition of bathymetric data for GIS applications. *Int. Arch. Photogramm. Remote Sens. Spat. Inf. Sci 40*: 123.

Hanjianga, X., Limina, T., Longa, S., 2008. A strategy to build a seamless multi-scale TIN-DEM database. *Int. Arch. Photogramm. Remote Sens. Spat. Inf. Sci 37*.

Hutchinson, M.F., Xu, T., Stein, J.A., 2011. Recent progress in the ANUDEM elevation gridding procedure. Geomorphometry 2011, 19–22.

INEGI, 2016. Continuo de Elevaciones Mexicano 3.0 (CEM 3.0) [WWW Document]. Datos Relieve. URL http://www.inegi.org.mx/geo/contenidos/datosrelieve/continental/continuoelevaciones.aspx (accessed 3.16.16).

INEGI, 2015. El geoide gravimétrico mexicano 2010. Instituto Nacional de Estadística y Geografía, México.

Isiorho, S.A., Matisoff, G., Wehn, K., 1996. Seepage relationships between Lake Chad and the Chad aquifers. *Groundwater 34*: 819–826.

Jensen, J.R., 2007. Remote Sensing of the Environment: An Earth Resource Perspective 2/e, 2nd ed, Prentice Hall Series. Pearson Education.

Johnson, B.A., Tateishi, R., Hoan, N.T., 2012. Satellite image pansharpening using a hybrid approach for object-based image analysis. *ISPRS Int. J. Geo-Inf 1*: 228–241.

Knott, S.T., Hersey, J.B., 1957. Interpretation of high-resolution echo-sounding techniques and their use in bathymetry, marine geophysics, and biology. *Deep Sea Res 1953 (4)*: 36–44.

Kottek, M., Grieser, J., Beck, C., Rudolf, B., Rubel, F., 2006. World map of the Köppen-Geiger climate classification updated. *Meteorol. Z. 15,* 259–263.

Krause, D., Menard, H., 1965. Depth distribution and bathymetric classification of some sea-floor profiles. *Mar. Geol. 3*, 169–193.

Leon, J.X., Cohen, T., 2012. An improved bathymetric model for the modern and palaeo Lake Eyre. *Geomorphology* 173, 69–79.

Lillesand, T., Kiefer, R.W., Chipman, J., 2014. Remote sensing and image interpretation. John Wiley & Sons.

Lu, S., Ouyang, N., Wu, B., Wei, Y., Tesemma, Z., 2013. Lake water volume calculation with time series remote-sensing images. *Int. J. Remote Sens. 34*, 7962–7973.

Ma, M., Wang, X., Veroustraete, F., Dong, L., 2007. Change in area of Ebinur Lake during the 1998–2005 period. *Int. J. Remote Sens. 28*, 5523–5533.

McFeeters, S.K., 1996. The use of the Normalized Difference Water Index (NDWI) in the delineation of open water features. *Int. J. Remote Sens. 17*, 1425–1432.

McPherson, K.R., Freeman, L.A., Flint, L.E., 2011. Analysis of methods to determine storage capacity of, and sedimentation in, Loch Lomond Reservoir, Santa Cruz County, California, 2009 (USGS Numbered Series No. 2011–5141), Scientific Investigations Report. U.S. Geological Survey, Reston, VA.

Mi, H., Zai, J., Jiang, X., 2007. Contrast and Analysis of Reservoir Storage Calculation Methods [J]. Surv. Mapp. Geol. Miner. Resour. 2,000.

NASA, 2017. History Landsat Science [WWW Document]. URL https://landsat.gsfc.nasa.gov/about/history/ (accessed 9.1.17).

Popielarczyk, D., Templin, T., 2014. Application of integrated GNSS/hydroacoustic measurements and GIS geodatabase models for bottom analysis of Lake Hancza: the deepest inland reservoir in Poland. *Pure Appl. Geophys. 171*, 997–1011.

QGIS Development Team (2018). QGIS Geographic Information System. Open Source Geospatial Foundation Project. http://qgis.osgeo.org

Rana, H., Neeru, N., 2017. Water Detection using Satellite Images Obtained through Remote Sensing. *Adv. Comput. Sci. Technol. 10*, 1923–1940.

Rojas-Villalobos, H.L., 2016. 3D bathymetric model of a shallow lagoon measured by a solar powered low-cost autonomous surface vehicle prototype in Cuauhtémoc, Chihuahua, Mexico. (Academic Research), Student Water Research Awards 2015-2016. New Mexico Water Resources Research Institute, Las Cruces, NM.

Ruddick, K.G., De Cauwer, V., Park, Y.-J., Moore, G., 2006. Seaborne measurements of near infrared water-leaving reflectance: The similarity spectrum for turbid waters. *Limnol Ocean. 51*, 1167–1179.

Schmitt, T., Mitchell, N.C., Ramsay, A.T.S., 2008. Characterizing uncertainties for quantifying bathymetry change between time-separated multibeam echo-sounder surveys. *Cont. Shelf Res. 28*, 1166–1176.

Servicio Meteorológico Nacional, 2017. Información Climatológica (1981-2010) [WWW Document]. URL http://smn.cna.gob.mx/es/informacion-climatologica-ver-estado?estado=chih (accessed 9.4.17).

USGS, 2017a. LandsatLook Viewer [WWW Document]. URL https://landsatlook.usgs.gov/ (accessed 8.22.17).

USGS, 2017b. SLC-off Products: Background | Landsat Missions [WWW Document]. URL https://landsat.usgs.gov/slc-products-background (accessed 8.28.17).

Winter, T.C., 1999. Relation of streams, lakes, and wetlands to groundwater flow systems. *Hydrogeol. J. 7*, 28–45.

Xu, H., 2006. Modification of normalized difference water index (NDWI) to enhance open water features in remotely sensed imagery. *Int. J. Remote Sens. 27*, 3025–3033.

Este artículo es citado así:

Rojas-Villalobos, H. L., L. C. Alatorre-Cejudo, B. Stringam, Z. Samani, C. Brown. 2018. Topobathymetric 3D model reconstruction of shallow water bodies through remote sensing, GPS, and bathymetry. *Tecnociencia Chihuahua 12(1)*:42-54.

DOI: https://doi.org/10.54167/tch.v12i1.129